
Beyond Accuracy and Alignment: A Diagnostic Evaluation Protocol for Feedback Alignment

Anonymous Author(s)

Affiliation

Address

email

Abstract

1 Modern feedback-alignment evaluation on deep residual networks is still summar-
2 ized by a deceptively simple pair: headline accuracy and headline cosine align-
3 ment Γ to the backpropagation gradient. We show that this pair can silently fail in
4 two distinct ways on standard CIFAR-10 pre-LayerNorm ResMLP and ViT-Mini
5 settings: first, *measurement degeneracy*, where residual-stream growth drives
6 hidden-layer BP gradients to the numerical floor and makes Γ uninterpretable;
7 and second, *low intrinsic credit-direction quality*, where random-feedback credit
8 remains essentially unaligned with BP on the deep blocks even when the reference
9 gradient is still meaningful. The headline result is that the field-standard reporting
10 pair walks back none of the methods we audit, whereas a four-diagnostic proto-
11 col walks back the three degenerate methods and passes the two trustworthy con-
12 trols. Intervention with a per-block scale-control penalty further reveals method-
13 dependent severity within the audited fixed-feedback family: State Bridge then
14 exceeds the architecture-matched frozen-blocks baseline by about 10 percentage
15 points, while Credit Bridge attains roughly $4\times$ DFA’s deep BP cosine yet matches
16 DFA’s accuracy—a dissociation that single-step nudging and integrated training-
17 loss decrease both confirm against the reverse cosine ordering, and that motivates
18 reporting layerwise credit quality jointly with a depth-utilization baseline. Our
19 contribution is an evaluation methodology paper for the NeurIPS 2026 Evaluations
20 & Datasets track: we provide the protocol, the calibration logic for its thresholds,
21 a reference implementation, a five-method audit, and validation through temporal
22 replay, cross-architecture checks, intervention-based disambiguation, and a docu-
23 mented catalog of pipeline pitfalls, in the spirit of critical evaluation analyses such
24 as Jordan et al. [3], O’Bray et al. [2], Paleka et al. [1].

25 1 Introduction

26 **Feedback alignment and the standard reporting pair.** Backpropagation (BP) is the de facto
27 training method for deep neural networks, but its requirement that each feedback connection carry a
28 weight identical to the corresponding forward connection – the weight-transport problem – has long
29 been considered biologically implausible [4, 8]. *Feedback alignment* (FA) [4] side-steps weight
30 transport by delivering per-layer credit through fixed random feedback matrices, and its direct vari-
31 ant (DFA) [5] projects the output error to every hidden layer through an independent random matrix;
32 parallel lines include target propagation [15] and equilibrium propagation [9]. These rules are stud-
33 ied both as biologically-plausible alternatives to BP and as scalable, asynchronous training schemes,
34 with recent work scaling DFA to transformer-scale architectures on language, recommendation, and
35 view-synthesis tasks [7, 6]. Evaluation in this line of work has converged on a two-number summary:

36 final task accuracy, and an aggregate cosine alignment Γ between the method’s per-layer credit and
37 the BP gradient on the trained network [4–8].

38 **The standard pair fails to validate.** On the audited 4-block $d=256$ ResMLP, however, Table 1
39 already shows that this accuracy-plus- Γ pair is not a validity check: DFA reaches only 0.306 ± 0.006
40 test accuracy, below the architecture-matched frozen-blocks baseline of 0.349 ± 0.002 , while still
41 looking superficially comparable to other non-BP methods. Figure 1 further shows that the apparent
42 cosine evidence is concentrated at the shallowest block, with DFA at seed 42 reaching about $+0.42$ at
43 layer 0 but approximately -0.03 to 0 on layers 1–4, so the aggregate obscures where credit direction
44 is and is not present. At the same time, the deepest BP reference norm is only about 4×10^{-10} for
45 DFA (three-seed mean) and a few $\times 10^{-9}$ for State Bridge and Credit Bridge, all below the 10^{-8}
46 clamp used by `F.cosine_similarity`, whereas BP remains around 4×10^{-4} , so the reported deep
47 cosine is partly computed against a numerical-floor reference rather than an informative gradient
48 direction (Figure 1; Table 1). Those numbers can be useful, but only if the measurement regime
49 itself is valid.

50 **Two failure modes and their separability.** Our audit shows that modern residual vision mod-
51 els can make these two quantities look informative while failing to answer the question they are
52 taken to answer. Figure 1 shows the first failure mode, which we call *Mode 1: measurement de-*
53 *generacy*, where residual-stream growth drives the deepest hidden state to about $\|h_L\| \sim 10^8$ under
54 DFA/SB/CB while the corresponding BP reference collapses to $\|g_L\| \sim 4 \times 10^{-10}$ for DFA (three-
55 seed mean), so the deep-layer cosine is measured against a clamp-dominated floor rather than a
56 meaningful target direction. The same figure also shows the second failure mode, *Mode 2: low*
57 *intrinsic credit-direction quality*, because even after comparing against the stronger frozen-blocks
58 baseline (0.349 ± 0.002) and looking layer-by-layer, DFA’s deep blocks remain essentially null
59 while only layer 0 is visibly positive. Intervention sharpens both modes. Adding a per-block resid-
60 ual penalty $\lambda \|f_i(h_i)\|^2$ to DFA at $\lambda=10^{-2}$ contains $\|h_L\|$ to about 4×10^4 and lifts the deep BP
61 reference to about 10^{-6} , but DFA’s rescued deep cosine is only about $+0.15$; State Bridge under the
62 same intervention reaches a three-seed deep cosine of $+0.32$ and, unlike DFA, exceeds the frozen-
63 blocks baseline by $+10$ points in final accuracy; Credit Bridge reaches a deep cosine near $+0.68$
64 yet matches only the DFA accuracy, so Mode 2 has method-dependent severity and deep cosine is
65 not a sufficient predictor of final accuracy across methods. At the same time, at $\lambda=10^{-4}$ Mode 1 is
66 alleviated while the DFA deep cosine still stays near zero, and at vanilla DFA epoch 1 the reference
67 is already meaningful at about 6×10^{-7} but the deep cosine is still -0.008 ± 0.013 across three
68 seeds. The failure is therefore neither unitary nor uniform: Mode 1 and Mode 2 are observationally
69 separable, and within the audited fixed-feedback family, the severity of each mode varies by method.

70 **Contribution: a methodology paper, not a new FA variant.** Accordingly, this paper does not
71 introduce a new FA variant or a new benchmark. Of the five methods we audit, BP, EP, and DFA are
72 established baselines from the published literature; the remaining two, which we call *State Bridge*
73 and *Credit Bridge*, are diagnostic probes we construct in this paper to directly learn the two targets
74 that different strands of the BP-free literature argue should produce good per-layer credit (formal
75 definitions and citations in Section 2). Instead, Table 1 and Figure 1 use a standard five-method
76 CIFAR-10 audit to show that status-quo reporting would treat BP, EP, DFA, State Bridge, and Credit
77 Bridge as the same kind of evidence-bearing object even though only BP and EP remain trustwor-
78 thy under matched diagnostic checks. This makes the contribution methodological in the sense of
79 Jordan et al. [3], O’Bray et al. [2], and Paleka et al. [1]: the central question is not whether one
80 more FA variant can post a headline number, but whether the reporting pipeline distinguishes mean-
81 ingful credit-direction evidence from numerical-floor artifacts and from shallow-only learning. The
82 protocol therefore starts from per-layer diagnostics and a frozen-blocks baseline before reading any
83 aggregate cosine or final accuracy as evidence about deep credit assignment. We first show the walk-
84 back on a standard audit, then isolate the two failure modes, and finally state the reporting protocol
85 that future FA papers should satisfy.

86 2 Audit: Standard Reporting Walks Back Nothing

87 **Setup: 5-method audit on a 4-block pre-LayerNorm ResMLP.** Table 1 fixes the canonical au-
88 dit to a 4-block pre-LayerNorm ResMLP with width $d=256$ on CIFAR-10, trained for 100 epochs

Table 1: Main audit table for the 4-block $d=256$ pre-LayerNorm ResMLP on CIFAR-10. The row and column structure is fixed here; fill from the three-seed audit output.

Method	Test acc.	Headline Γ	Status-quo verdict	Protocol verdict
BP	0.615 ± 0.003	≈ 1.0	trustworthy	trustworthy
EP	0.316 ± 0.030	0.008	trustworthy	trustworthy
DFA	0.306 ± 0.006	0.10	trustworthy	walked back
State Bridge	0.205 ± 0.032	0.005	trustworthy	walked back
Credit Bridge	0.289 ± 0.026	0.07	trustworthy	walked back

89 with AdamW (learning rate 10^{-3} , weight decay 0.01), a cosine schedule, batch size 128, and three
 90 seeds (42, 123, 456); all five methods are read against the identical architecture, optimizer, schedule,
 91 and training budget without method-specific tuning, and Figure 1 summarizes the corresponding
 92 per-block growth, deepest-layer BP reference norm, cross-batch stability, and frozen-baseline com-
 93 parison.

94 **State Bridge and Credit Bridge: diagnostic probes constructed for this paper.** Two rows in
 95 Table 1, *State Bridge* (SB) and *Credit Bridge* (CB), are diagnostic probes we construct in this paper,
 96 not prior FA variants. Each directly learns a target that a different strand of the BP-free literature
 97 argues should produce good per-layer credit, and each uses the same block local loss $-\langle f_l(h_l), a_l \rangle$
 98 as DFA but with a different a_l . SB instantiates the target-propagation view that accurate prediction
 99 of a downstream hidden state yields a usable credit signal [14, 15]: an auxiliary $G_\psi(h_l, t_l, s)$ is fit
 100 by MSE to predict h_L from $(h_l, t_l=l/L, s=e_T)$, and $a_l^{\text{SB}} = \nabla_{h_l} \text{CE}(W_{\text{out}} \text{LN}(G_\psi(h_l, t_l, s)), y)$.
 101 CB instantiates the synthetic-gradient view that a learned value network, if its input-gradient ap-
 102 proximates the BP gradient, can stand in for it [16]: $V_\phi(h_l, t_l, s)$ is fit via a bridge residual against
 103 an EMA target, and $a_l^{\text{CB}} = \nabla_{h_l} V_\phi(h_l, t_l, s)$. Both auxiliaries are trained on detached hidden states.
 104 We use SB and CB as controls that populate different points in the (angular agreement with BP, func-
 105 tional usefulness) plane; that is what makes the cross-method cosine-versus-accuracy dissociation
 106 in Section 4 visible.

107 **Status-quo reading: every method looks acceptable.** By the field’s usual criteria, the non-BP
 108 methods appear to train to nontrivial accuracy and report nonzero alignment. In Table 1, DFA
 109 reaches 0.306 ± 0.006 test accuracy with headline $\Gamma=0.10$, State Bridge reaches 0.205 ± 0.032 with
 110 $\Gamma=0.005$, and Credit Bridge reaches 0.289 ± 0.026 with $\Gamma=0.07$; none of these rows looks like
 111 an obvious invalidation if one is reading the usual pair of final accuracy and aggregate alignment
 112 in the style of prior FA reporting [4–7]. Even the absolute scale does not itself force a walk-back,
 113 because all three methods are plainly above chance and all three report positive headline alignment
 114 rather than a visibly broken or undefined quantity. That reading is exactly what the rest of the paper
 115 overturns.

116 **EP as the internal control: low accuracy without invalid measurement.** Low accuracy by itself
 117 is not the pathology. Equilibrium Propagation (EP), a contrastive energy-based alternative to BP that
 118 updates weights from the difference between a free-phase and a nudged-phase hidden trajectory, is
 119 the key internal comparison in Table 1 and Figure 1: it achieves only 0.316 ± 0.030 accuracy and a
 120 very small headline $\Gamma=0.008$, yet its three-seed mean max-per-block growth is only $6.6\times$ (highest
 121 single-seed value $11.0\times$), its deepest BP reference norm remains around 1.3×10^{-4} rather than
 122 collapsing to the numerical floor, and its cross-batch direction-stability score is 0.02 rather than the
 123 much higher drift-dominated values seen for DFA-family methods. At the same time, EP is not a
 124 positive result for depth usage in the stronger sense, because its trainable-model accuracy is still
 125 3.3 percentage points below the frozen-blocks baseline of 0.349 ± 0.002 . The distinction matters
 126 because it separates underperformance from invalid evaluation.

127 **Frozen-blocks baseline overturns the status-quo reading.** When we compare each method to a
 128 frozen-blocks baseline matched to the same architecture, the headline interpretation changes imme-
 129 diately. The frozen-blocks model, which trains only the embedding, LayerNorm, and head while
 130 holding the residual blocks fixed, reaches 0.349 ± 0.002 across the same three seeds; against that

5-method audit on 4-block $d=256$ ResMLP CIFAR-10 (3-seed mean \pm std)

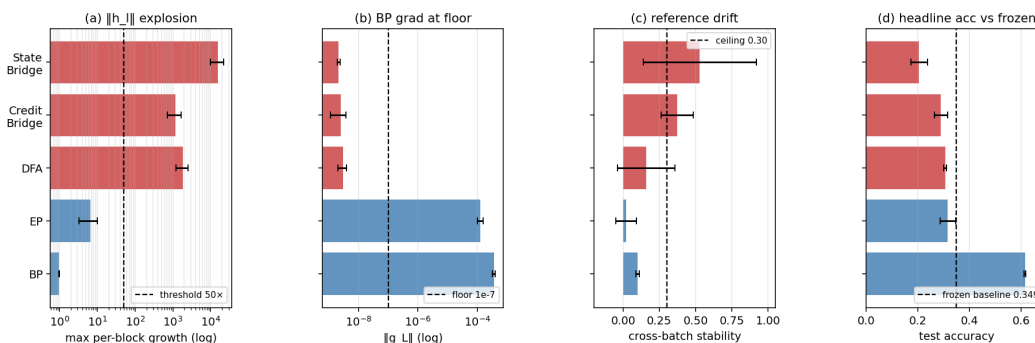


Figure 1: Five-method audit on the 4-block $d=256$ pre-LayerNorm ResMLP: the field-standard pair looks superficially consistent across methods, but the diagnostic view separates trustworthy controls from walked-back methods.

131 baseline, BP is higher by 26.6 points, but DFA is lower by 4.3 points, State Bridge by 14.4 points,
 132 Credit Bridge by 6.0 points, and even EP by 3.3 points. Figure 1 shows that this accuracy compari-
 133 son lines up with the diagnostic split: DFA, State Bridge, and Credit Bridge also combine extreme
 134 per-block growth (three-seed mean max ratios $\sim 1.9 \times 10^3$, $\sim 1.6 \times 10^4$, and $\sim 1.2 \times 10^3$ respec-
 135 tively), deepest-layer BP norms around 10^{-9} , and high cross-batch instability (0.16, 0.53, and 0.37),
 136 so their deep blocks are at best passengers and in practice often harmful. This establishes the audit
 137 question the rest of the paper must answer: why do the standard signals fail so badly?

138 3 Failure Mode 1: Measurement Degeneracy

139 **The two parts of Mode 1.** Mode 1 has two parts. The activation-growth part (a) is a scale pathol-
 140 ogy of fixed-feedback local-credit objectives without an effective scale-control term: for block l ,
 141 DFA, State Bridge, and Credit Bridge each update f_l by maximizing a local objective of the form
 142 $\langle f_l(h_l), a_l \rangle$, where the per-layer credit vector a_l is the method-specific projection of the output
 143 error (for DFA, $a_l = B_l^\top e_T$ with a fixed random B_l ; for State Bridge, a_l is the gradient of a cross-
 144 entropy loss measured through a learned state predictor $G_\psi(h_l, t_l, s)$ that estimates h_L ; for Credit
 145 Bridge, a_l is the gradient of a learned value network $V(h_l, t_l, s)$). None of these three local losses
 146 contains a penalty on $\|f_l(h_l)\|$, so any direction in which a larger block output improves inner-
 147 product alignment with the method’s fixed or learned credit target is rewarded; in a pre-LN residual
 148 stack, larger block outputs directly increase residual-stream scale, and terminal LayerNorm at the
 149 output removes task-loss sensitivity to that scale, so the architecture supplies no global restraint on
 150 the local growth incentive. The gradient-floor part (b) follows from the LayerNorm Jacobian. For
 151 $y = \text{LN}(h) = (h - \mu(h))/\sigma(h)$ with $\sigma(h) = (\frac{1}{d} \sum_i (h_i - \mu(h))^2)^{1/2}$ proportional to $\|h\|/\sqrt{d}$,
 152 the spectral norm of $\partial y/\partial h$ is $\Theta(1/\sigma(h))$, so back-propagating through terminal LayerNorm scales
 153 the deepest hidden BP gradient as $\|g_L\| = \Theta(1/\|h_L\|)$, and the same residual-stream inflation that
 154 drives diagnostic (a) drives a proportional collapse of the diagnostic (b) reference. Empirically, on
 155 the audited 4-block pre-LayerNorm ResMLP ($d=256$, CIFAR-10, 100 epochs, 3 seeds), DFA train-
 156 ing drives the three-seed mean $\|h_L\|$ from about 9 at initialization to about 5×10^8 by epoch 100
 157 and $\|g_L\|$ from about 9.8×10^{-4} to about 4×10^{-10} , while the reported deep cosine remains defined
 158 only because `F.cosine_similarity` clamps the denominator at $\varepsilon=10^{-8}$ (Table 1; Figure 1). At
 159 that endpoint the reference norm is about $25\times$ below the clamp, so the quantity being reported is
 160 effectively $(a \cdot b)/(\|a\| \max(\|b\|, 10^{-8}))$ rather than a comparison to a meaningful BP direction.

161 **Falsification chain: four alternative attributions.** We tested this mechanism story against four
 162 natural alternative attributions, all of which it survives. *Not residual-skip-driven:* with terminal
 163 LN kept and the additive skip removed ($h_{l+1}=F_l(h_l)$), DFA still converges across three seeds
 164 to mean $\|h_L\| \approx 8.2 \times 10^7$ and mean $\|g_L\| \approx 1.9 \times 10^{-10}$ at 100 epochs, both at the diagnostic floor
 165 (Appendix H). *Not task-signal-driven:* under i.i.d. random class targets per minibatch, DFA still

reaches $\|h_L\| \approx 1.67 \times 10^8$ and $\|g_L\| \approx 8 \times 10^{-12}$ while accuracy stays at chance (Appendix I). *Not DFA-specific*: the same random-target ablation drives $\|h_L\|$ to 6.2×10^3 for SB and 2.0×10^4 for CB in three epochs, so all three audited fixed-feedback methods exhibit data-agnostic activation growth. *Not shared by EP*: under the same protocol, EP keeps $\|h_L\| \approx 586$ at five epochs, $25 \times$ smaller than DFA’s three-epoch value, confirming that the random-target assay separates the explosion-prone fixed-feedback class from EP’s energy-based objective.

Causal control: removing terminal LayerNorm on the same backbone. The matched same-backbone causal control for diagnostic (b) is removing terminal LayerNorm. On the same ResMLP-d256 with the residual skip intact, 100 epochs of DFA, three seeds, the residual stream still inflates to $\|h_L\| \approx 1.21 \times 10^7$, but the deepest hidden-layer BP gradient remains at $\|g_L\| \approx 7.2 \times 10^{-4}$ (four orders of magnitude above the diagnostic (b) floor), and the final test accuracy is 0.327 ± 0.012 , statistically indistinguishable from vanilla DFA’s 0.306 ± 0.006 on the same backbone with terminal LayerNorm intact. Removing terminal LayerNorm therefore preserves Mode 1 (a) but cleanly eliminates Mode 1 (b) on the same architecture, while leaving final task accuracy essentially unchanged. Combined with the broader cross-architecture pattern (the no-terminal-LN ResMLP-d256 ablation and the BatchNorm CNN, which lack terminal LayerNorm, never trigger diagnostic (b); ViT-Mini with a terminal LN does, by epochs 2–3 (Figure 3)), terminal LayerNorm is necessary for Mode 1 (b) in the audited residual ResMLP and ViT-Mini setting. The collapse is also not a late-epoch curiosity: $\|g_L\|$ drops from 9.8×10^{-4} at epoch 0 to 5.8×10^{-8} by epoch 4 in the three-seed temporal replay (per seed: 6.8, 6.4, 4.1×10^{-8}), so the protocol fires within the first 11 epochs of a 100-epoch run and is actionable as an early-stop criterion rather than a post hoc explanation. Once measurement degeneracy is identified, the next question is whether poor deep credit remains even before collapse.

4 Failure Mode 2: Low Intrinsic Credit-Direction Quality

Mode 2 is present even when measurement is meaningful. The second failure mode appears even in the meaningful-measurement regime. At the earliest vanilla DFA checkpoints on ResMLP, the hidden backpropagated gradient at the first deep block remains above the numerical floor: at epoch 1, $\|g_2\|$ is 6.8×10^{-7} , 6.6×10^{-7} , and 3.8×10^{-7} across the three seeds, all above the 10^{-7} threshold used to distinguish measurable from collapsed gradients. Yet the corresponding deep-layer cosine values are already essentially null: across layers 1–4, all seed-level measurements at epoch 1 lie in $[-0.04, +0.02]$, with a three-seed mean of -0.008 ± 0.013 , and by epoch 2 the deep mean is still only -0.018 ± 0.018 (Table 2). This is the observational pattern predicted by low credit-direction quality rather than mere disappearance of signal: the gradient is still present enough to measure, but the directions delivered to the deep network carry little agreement with backpropagation, consistent with prior concerns that alternative feedback rules can fail by supplying poor credit assignments even before full collapse [8, 10, 12, 11]. This rules out the simplest objection that the deep-layer null result is merely a byproduct of collapse.

A second metric with different failure modes agrees. A second metric with different numerical failure modes tells the same story. Cosine measures directional agreement with the BP gradient, whereas the per-layer perturbation correlation ρ_l measures whether the proposed credit predicts the actual loss response: for $M=32$ unit-norm random directions v_m and step $\varepsilon=10^{-3}$, $\rho_l = \text{Pearson}_m(\langle a_l, \varepsilon v_m \rangle, \ell(h_l + \varepsilon v_m) - \ell(h_l))$, evaluated per sample on a fixed eval batch and then averaged. Cosine and ρ have different failure modes, especially with respect to normalization and small-denominator effects. In our controls, ρ behaves as expected, with a Taylor-ceiling positive control near $+0.997$ and a random-vector negative control near $+0.006$ (Figure 4, Table 2). On vanilla DFA, deep ρ is likewise null: for the early checkpoints where the gradients remain measurable, the deep average is -0.003 ± 0.005 across seeds and epochs, and in a floor-level checkpoint it is $+0.002$, again indistinguishable from noise. The agreement between cosine and ρ therefore rules out the interpretation that the null deep result is an artifact of cosine’s ε -clamp or vector normalization. The deep blocks are not just hard to measure; they are receiving weakly useful directions.

Per-layer reporting is mandatory: layer-0 dominance. Per-layer reporting is therefore not cosmetic. In ResMLP under vanilla DFA, the headline aggregate alignment $\Gamma \approx 0.07$ – 0.10 can look mildly positive only because layer 0 remains strongly aligned while the deep network is not: at the same epoch-1 checkpoints where layers 1–4 are essentially zero, layer 0 has cosine $+0.42$, $+0.44$,

219 and +0.42 across seeds (Table 2; per-seed values in Appendix K). The resulting average can there-
 220 fore be driven by the embedding layer even when the interior blocks are effectively unaligned, so
 221 aggregate reporting obscures the very distinction needed to separate “measurement collapse” from
 222 “poor credit direction.” This layer-0 dominance is specific to the ResMLP DFA setting; on ViT-Mini
 223 DFA, all layers are near zero, which strengthens the broader methodological point that alignment
 224 should be reported per layer rather than only in aggregate. With the two modes separated observa-
 225 tionally, the remaining question is whether intervention can move them independently.

226 **Method-dependent severity once Mode 1 is alleviated.** Mode 2 has method-dependent severity
 227 within the audited fixed-feedback family once Mode 1 is alleviated. Applying the same $\lambda=10^{-2}$
 228 scale-control penalty to SB, CB, and DFA on the audited 4-block $d=256$ ResMLP for 30 epochs
 229 (three seeds) gives, in order, test accuracies 0.453 ± 0.003 , 0.360 ± 0.003 , 0.360 ± 0.001 and deep
 230 mean cosines $+0.322 \pm 0.007$, $+0.679 \pm 0.008$, $+0.151 \pm 0.025$ (deep mean ρ $+0.402$, $+0.464$,
 231 $+0.080$ and full $\|h_L\|/\|g_L\|$ in Appendix J), all in the meaningful-measurement regime. SB+penalty
 232 is the first audited non-BP method whose trained deep blocks beat the frozen-blocks baseline (0.349),
 233 by +10.4 pp—comparable to BP+penalty’s +18.3 pp.

234 **Three functional metrics rank the methods consistently; cosine disagrees.** Within this rescued
 235 regime the three methods reveal a clean cosine-versus-accuracy dissociation, and two independent
 236 functional measurements rule out the interpretation that cosine is just noisy. *Nudging*: a single step
 237 $\eta=0.01$ along each method’s per-layer credit a_l at the converged checkpoint changes the deep-block
 238 test loss by $-1.93 \pm 0.11 \times 10^{-3}$ (SB+pen), $-4.26 \pm 0.24 \times 10^{-4}$ (CB+pen), and $-4.98 \pm 0.44 \times$
 239 10^{-5} (DFA+pen) across three seeds (per-seed values in Appendix J): SB moves the loss $\approx 4.5\times$
 240 more than CB and $\approx 39\times$ more than DFA, even though CB has the highest deep cosine with BP.
 241 *Training-loss trajectory*: the integrated 30-epoch training loss decrease across three seeds ranks SB
 242 $(-0.447 \pm 0.008) \gg$ CB $(-0.121 \pm 0.003) \approx$ DFA (-0.095 ± 0.007) . All three functional metrics
 243 (accuracy, nudging, training-loss trajectory) agree on SB \gg CB \approx DFA; the deep-cosine ordering
 244 CB $>$ SB $>$ DFA is the only one that disagrees (Figure 2).

245 **A three-part proposition: observation, inference, mechanism hypothesis.** We frame the
 246 Mode 2 reading as a three-part proposition. *Observation*: under the same intervention and budget,
 247 CB has $4\times$ DFA’s deep cosine yet matches DFA’s accuracy, while SB attains the best accuracy with
 248 intermediate cosine; the same SB \gg CB \approx DFA ranking is reproduced by single-step nudging and
 249 30-epoch training-loss decrease. *Inference*: layerwise cosine is necessary to rule out grossly wrong
 250 credit signals—it cleanly distinguishes the rescued regime from the clamp-dominated vanilla regime
 251 where deep cos is essentially zero—but it is not sufficient to certify that the supplied signal is useful
 252 credit for depth, because three independent functional metrics rank the same three methods in the
 253 opposite order from cosine. *Mechanism hypothesis*: usefulness depends on whether the local update
 254 induces useful forward-state change across blocks, not merely on the angle between the local credit
 255 direction and the BP gradient. Under this reading, CB supplies a gradient-direction surrogate that
 256 aligns in angle without translating into coordinated forward-state improvement, while SB supplies
 257 a state-level teaching signal that preserves aspects of useful credit which layerwise cosine does not
 258 measure. The single-step nudging test and the integrated training-loss decrease are direct functional
 259 probes of exactly this distinction: they measure what an actual descent step in the proposed credit
 260 direction does to the loss, rather than how the direction angle compares to the BP gradient at one
 261 frozen point.

262 **Mode 1 may be a downstream symptom of Mode 2.** The same mechanism story suggests a
 263 causal reading of the relationship between the two failure modes: that Mode 1 is plausibly a down-
 264 stream symptom of Mode 2 rather than a parallel, independent failure. The reasoning is constructive.
 265 Each fixed-feedback method’s local objective is the inner product $\langle f_l(h_l), a_l \rangle$, with no penalty on
 266 $\|f_l\|$. If the credit vector a_l does not point along a direction in which a small change of the resid-
 267 ual contribution f_l produces useful forward-state improvement (Mode 2), then the only remaining
 268 way for the optimizer to keep increasing the inner product is to inflate $\|f_l\|$ in the direction set by
 269 the random a_l , since that is the cheap path for which the architecture supplies no global restraint.
 270 Inflating $\|f_l\|$ directly produces the activation-growth signature of Mode 1(a), and via the LN Jaco-
 271 bian relation $\|g_L\| = \Theta(1/\|h_L\|)$ derived in Section 3 it then drives the gradient-floor collapse of
 272 Mode 1(b). The per-block penalty $\lambda\|f_l\|^2$ breaks this chain at the inflation step by adding an explicit
 273 cost to growing $\|f_l\|$, which contains $\|h_L\|$ and lifts $\|g_L\|$ above the diagnostic floor without ever

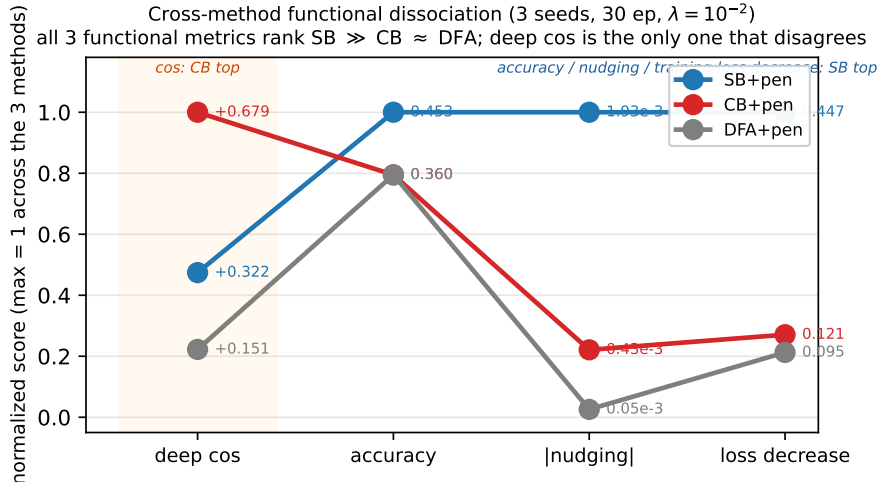


Figure 2: Cross-method functional dissociation under matched penalty rescue ($\lambda=10^{-2}$, 30 epochs, 3 seeds, 4-block $d=256$ pre-LayerNorm ResMLP). Each line tracks one method across four metrics, normalized so that the maximum across methods equals 1.0 in each column; raw values are annotated. Deep cosine to the BP gradient ranks the three methods $CB>SB>DFA$, but the three functional metrics (test accuracy, single-step nudging-test loss decrease, and integrated 30-epoch training-loss decrease) all rank them $SB\gg CB\approx DFA$. The X-pattern between deep cos and accuracy is the cross-method cos-versus-accuracy dissociation: SB rises from middle (cos) to top (functional), CB drops from top (cos) to tied with DFA (functional). Deep cosine is the only one of the four metrics that does not predict accuracy.

274 modifying the underlying credit-direction quality of a_l . This explains the otherwise-asymmetric ob-
275 servation that the same intervention alleviates Mode 1 (a)+(b) cleanly while leaving Mode 2 only
276 partially addressed: the penalty addresses the symptom, not the cause.

277 **Hypothesis status and reporting rule.** We state this as a hypothesis rather than a theorem for two
278 reasons. First, we have measured the angle-to-accuracy gap and two functional proxies (nudging
279 and training-loss decrease) but not the full per-block forward-state-change content over training.
280 Second, the data is also formally consistent with a parallel-failure-mode reading in which Mode 1
281 and Mode 2 are independently destructive and the penalty happens to address Mode 1 only; nothing
282 in the audit forces the downstream-of-Mode 2 reading over this alternative. The reporting rule that
283 follows is robust to either interpretation: if Mode 1 is downstream then the penalty addresses a
284 symptom and the lower-bound credit-quality gap is the dominant residual, while if the modes are
285 parallel then the penalty addresses Mode 1 only and Mode 2 remains an additive deficit; in both cases
286 the cross-method dissociation between deep cosine and the three functional metrics strengthens the
287 methodological point that alignment must be reported jointly with measurement validity and a depth-
288 utilization baseline rather than as a single headline number.

289 5 Intervention and Cross-Architecture Evidence

290 **The penalty rescues the measurement regime.** The penalty intervention first matters as a rescue
291 of the measurement regime. When we add a per-block penalty $\lambda \text{mean}(\|f_l(h_l)\|^2)$ to DFA’s local
292 loss and train the 4-block $d=256$ ResMLP for 30 epochs on CIFAR-10, the $\lambda=10^{-2}$ setting contains
293 the terminal hidden-state scale from $\|h_L\| \sim 4.4 \times 10^8$ under vanilla DFA to $\sim 4.0 \times 10^4$, while
294 lifting the deepest BP reference norm from $\|g_L\| \sim 5 \times 10^{-10}$ to $\sim 9.0 \times 10^{-7}$, a roughly four-order-
295 of-magnitude rescue on both quantities (Figure 4; Table 2). At that setting, both diagnostic (a) and
296 diagnostic (b) pass on penalized DFA, and test accuracy rises to 0.360 ± 0.001 from 0.301 ± 0.005 for
297 matched 30-epoch vanilla DFA. The key point is not yet that the recovered network has good deep
298 credit, but that the deep reference vector is again large enough to function as a meaningful target
299 direction rather than a clamp-dominated artifact. That rescue makes the second question measurable
300 rather than hypothetical.

Table 2: Two-mode validation table built around the intervention and disambiguation results.

Condition	Deep-layer alignment signal	Measurement regime	Interpretation
Vanilla DFA, early epoch	$\overline{\text{cos}}_{deep} = -0.008 \pm 0.013, \overline{\rho}_{deep} = -0.003 \pm 0.005$	meaningful ($\ g\ \sim 10^{-6}$)	mode 2 present without mode 1
Vanilla DFA, converged	$\overline{\text{cos}}_{deep} = -0.022, \overline{\rho}_{deep} = +0.002$	degenerate ($\ g\ \sim 10^{-9}$)	mode 1 obscures mode 2
Penalized DFA, $\lambda = 10^{-2}$	$\overline{\text{cos}}_{deep} = +0.151 \pm 0.025, \overline{\rho}_{deep} = +0.080 \pm 0.011$	meaningful ($\ g\ \sim 10^{-6}$)	partial alleviation of both modes
Fresh- B null control	$\overline{\text{cos}}_{deep} = +0.002 \pm 0.022$ ($n=20$ draws)	meaningful	training-specific adaptation check

301 **Penalty alleviates Mode 2 only partially; the λ sweep separates the modes.** Once the reference
302 vector is meaningful again, the deep layers no longer sit exactly at null. At $\lambda=10^{-2}$, penalized DFA
303 reaches a three-seed deep-layer mean cosine of $+0.151 \pm 0.025$ and deep perturbation correlation
304 of $+0.080 \pm 0.011$, whereas vanilla DFA is essentially zero on both metrics in the deep blocks,
305 consistent with prior concerns that alternative feedback can fail by supplying poor credit directions
306 even before full collapse [8, 10, 12, 11]. The null calibration rules out the interpretation that this
307 recovered signal is merely measurement noise: on the same penalized checkpoint, replacing the
308 training-time feedback matrices with 20 fresh random B_i draws gives a deep cosine of only $+0.002 \pm$
309 0.022 , with per-layer standard deviations of 0.013 – 0.023 , all within noise of zero (Table 2). The λ
310 sweep sharpens the dissociation further: at $\lambda=10^{-4}$, Mode 1 is already alleviated, with three-seed
311 mean $\|h_L\| \approx 2.2 \times 10^4$ and $\|g_L\| \approx 7.0 \times 10^{-7}$, but the three-seed deep cosine remains -0.020 , while
312 $\lambda=10^{-2}$ delivers the $+0.151$ and $+0.080$ above (Figure 4). The improvement is real, but it is only
313 partial.

314 **Capacity-cost control: BP under the same penalty.** A rescue intervention is only informative if
315 its direct cost is controlled. The relevant control is BP trained under the same penalty for the same
316 matched 30-epoch budget: across three seeds, BP falls from 0.585 ± 0.001 without the penalty to
317 0.532 ± 0.006 with $\lambda=10^{-2}$, so the penalty has a direct cost of about 5.3 percentage points even
318 when credit assignment is correct, whereas DFA moves in the opposite direction, from 0.301 ± 0.005
319 to 0.360 ± 0.001 , and State Bridge moves further still, from 0.213 to 0.453 ± 0.003 , all under
320 the same 30-epoch intervention (Figure 4; Appendix J). Relative to the frozen-blocks baseline of
321 0.349 , BP+penalty retains a margin of $+18.3$ points, State Bridge+penalty retains $+10.4$ points, and
322 DFA+penalty retains only $+1.1$ points. The remaining BP-to-DFA gap of 17.2 points is therefore
323 a lower bound on the part of DFA’s deficit that is not explained by simple penalty-induced capacity
324 loss alone, though not a clean isolation because BP uses an end-to-end loss whereas DFA uses block-
325 local losses. The substantially smaller BP-to-State-Bridge gap of $0.532 - 0.453 = 7.9$ points shows
326 that the cross-method differences in penalty-rescued accuracy are not all attributable to a uniform
327 “random-feedback ceiling”: the bridge construction in State Bridge can recover much more of the
328 BP-with-penalty performance than DFA can, on the same architecture and the same intervention.
329 The residual gap after that control is what keeps Mode 2 substantively alive while letting it have
330 method-dependent severity.

331 **Cross-architecture and depth-sweep evidence.** The architecture comparison sharpens the scope
332 of the critique. In the terminal-LN architectures we audited, both diagnostics fire for DFA-trained
333 ResMLP at $d=256$, the same pattern recurs at $d=512$ with even larger max-per-block growth (DFA
334 three-seed mean about 7×10^3 vs $\sim 1.9 \times 10^3$ at $d=256$), and ViT-Mini with a class token and
335 terminal LN shows diagnostic (a) by epoch 1 and diagnostic (b) by epochs 2–3 (Figure 3). A depth
336 sweep on the $d=512$ ResMLP at $L \in \{2, 4, 6, 8, 12\}$ shows that the layerwise pattern is essentially
337 depth-invariant: DFA’s layer-0 cosine stays in $[+0.38, +0.40]$ across all five depths, while its mean
338 deep-layer cosine stays within $[-0.005, +0.000]$ and its deep perturbation correlation collapses to
339 0.000 in every depth tested, even though BP retains a deep-layer cosine of $+0.94$ at $L=12$ (Ap-
340 pendix G). The deep credit signal does not improve when the network is shallower, so the failure is
341 not a “too deep” artifact. In the non-terminal-LN controls, the pattern is different: the no-terminal-
342 LN ResMLP-d256 ablation shows diagnostic (a) firing across three seeds at epochs $\{18, 14, 25\}$ but
343 diagnostic (b) never fires across 100 epochs and the same three seeds, and the BatchNorm CNN on
344 CIFAR-10 likewise shows strong growth under DFA, with max-per-block growth up to $237\times$, but
345 keeps deepest BP gradients around $\|g\| \sim 10^{-3}$ and never triggers diagnostic (b) (Figure 3). BP
346 never triggers either diagnostic in any audited architecture. The matched same-backbone ResMLP-
347 d256 ablation in Section 3 supplies the cleanest causal control: removing terminal LayerNorm from
348 the same architecture preserves activation growth but eliminates the gradient floor, so diagnostic (b)
349 is necessary on terminal-LN ResMLP and is not just an architecture-class coincidence. The broader

Cross-architecture temporal evolution of FA diagnostics (seed 42)

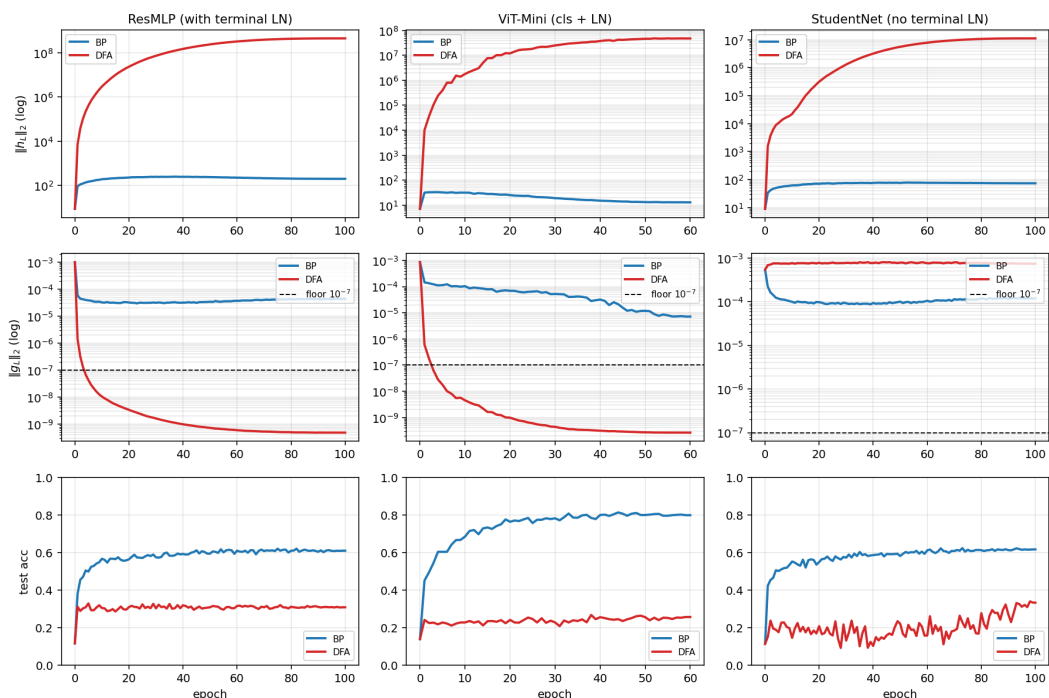


Figure 3: Temporal and cross-architecture validation: the protocol fires early on terminal-normalized residual architectures, never fires on BP controls, and separates the activation-growth pathology from the gradient-floor pathology.

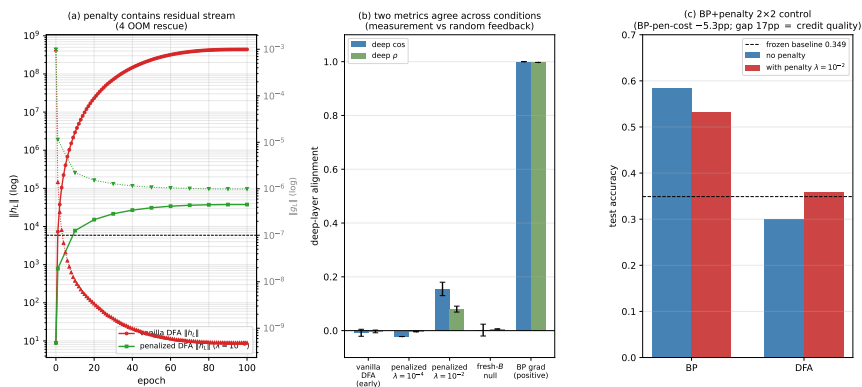


Figure 4: Penalty intervention view of the two modes: penalization rescues residual-stream scale and restores a measurable but still partial deep-layer credit signal, clarifying that numerical rescue and credit-quality rescue are related but distinct.

350 claim therefore holds at full strength inside the audited residual ResMLP and ViT-Mini regime, while
 351 diagnostic (a) remains useful more broadly. This lets the paper end with a reporting rule rather than
 352 an overclaimed theory.

353 6 Recommended FA Evaluation Protocol

354 **Start from measurement validity.** The reporting protocol begins with measurement validity. Be-
 355 fore any FA paper reports a headline alignment number, it should report per-layer state scale and

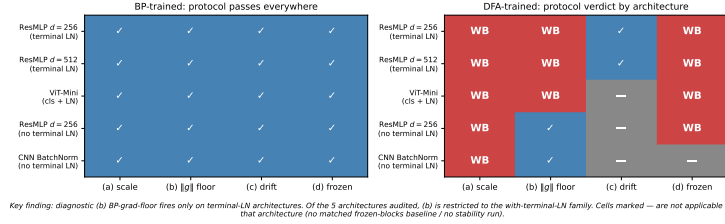


Figure 5: Cross-architecture summary over ResMLP, ViT-Mini, no-terminal-LN ResMLP, and CNN: activation-growth failures recur across architectures, while gradient-floor failures appear in the terminal-normalized settings audited here.

Table 3: Protocol definition table. Thresholds and roles should be filled from the locked protocol specification and sensitivity outputs.

Diag.	Measurement	Default threshold	Role
(a)	Per-layer activation scale via max-per-block growth $\max_i \ h_{l+1}\ /\ h_l\ $	$> 50\times$	binary detector
(b)	Deepest hidden-layer BP gradient norm $\ g_L\ $	$< 10^{-7}$	binary detector
(c)	Cross-batch direction stability of normalized BP gradients	> 0.30	sub-mode discriminator
(d)	Frozen-blocks baseline margin for trained blocks over random blocks	$< 2\text{pp}$	depth-utilization check

356 the hidden BP reference-gradient scale at the layers where the scientific claim is being made. In our
357 audited regime, those two quantities already separate healthy from invalid measurement with unusu-
358 ally wide margins: the maximum per-block growth stays below about $11\times$ for BP and EP but is at
359 least $694\times$ for the degenerate methods, giving a $63\times$ calibration gap, while the deepest hidden BP
360 norm stays above about 10^{-4} for BP and EP but below about 4×10^{-9} for the degenerate methods,
361 giving a $24,338\times$ gap (Table 3; Table 1; Figure 5). These are not cosmetic diagnostics around the
362 real result: they determine whether the reported cosine is being computed against an informative BP
363 direction or against a floor-level reference. If the reference gradient is at floor, the evaluator should
364 stop treating aggregate alignment as evidence.

365 **Decision value: which diagnostics actually walk back which methods.** The point of the proto-
366 col is not to add plots; it is to prevent a specific class of false conclusions. For this paper, the minimal
367 protocol is four checks: per-layer activation scale via max-per-block growth, deepest hidden BP gra-
368 dient floor, meaningful-regime per-layer credit quality, and an architecture-matched frozen-blocks
369 baseline (Table 3). The first two ask whether the reference quantity is still valid; the third asks
370 whether, once validity is restored, the deep blocks receive useful directions; and the fourth asks
371 whether the trained depth is doing better than a model whose residual blocks were never trained
372 at all. Figure 6 (Appendix D) makes the decision value explicit: accuracy alone walks back 0/5
373 audited methods, accuracy plus headline Γ still walks back 0/5, and the full protocol walks back
374 3/5 by flagging DFA, State Bridge, and Credit Bridge, with diagnostics (a), (b), and (d) each inde-
375 pendently sufficient for binary detection on those failures. On our audit, these checks catch failures
376 that accuracy plus aggregate alignment miss completely.

377 **Diagnostic roles and calibration.** The protocol is conservative in a specific sense: it preserves
378 BP and EP as evidence-bearing controls and walks back only claims that fail measurement-validity
379 or depth-utilization checks. Diagnostics (a) and (b) have sharp empirical calibration gaps in the
380 audited regime (Appendix E), diagnostic (c) is a sub-mode discriminator computed as the mean
381 pairwise cosine of the per-batch-averaged BP-grad direction at the chosen layer across $K \geq 8$ dis-
382 joint 128-sample minibatches (in our 5-method audit, healthy methods cluster near zero with all six
383 BP/EP values in $[-0.04, +0.12]$, while drift-dominated cases reach high tails up to $+0.99$, and 5/9
384 degenerate values exceed the 0.30 default cutoff), and diagnostic (d) uses a deliberately weak 2pp
385 margin as a context check rather than a theorem about useful depth. The Section 4 cross-method
386 cosine-versus-accuracy dissociation reinforces the necessity of keeping all four diagnostics separate:
387 Credit Bridge, State Bridge, and DFA differ by more than $4\times$ in deep-layer alignment under the
388 same penalty rescue without tracking final accuracy in the same direction, so aligning an alternative
389 credit rule with the BP gradient is not a substitute for checking depth utilization against a matched
390 shallow baseline.

391 7 Discussion, Limits, Conclusion

392 **Scope, limits, and reporting recommendation.** Our claim is about evidence, not impossibility:
393 we show that current FA evaluation practice can misread what happened, not that FA cannot
394 work in deep networks. DFA, SB, and CB all pass status-quo reporting (Table 1) but fail the
395 protocol’s deep checks, and the Figure 4 penalty partially rescues credit signal rather than validating
396 headlines. Our strongest claim is scoped to $d=256/512$ pre-LayerNorm ResMLPs and ViT-Mini,
397 where both Mode 1 diagnostics fire; the no-terminal-LN ResMLP ablation establishes terminal
398 LayerNorm as causally necessary for diagnostic (b) on residual ResMLP and (with the BatchNorm
399 CNN) shows that activation growth can persist without gradient-floor collapse; the dataset is
400 CIFAR-10; and the BP-plus-penalty comparison is a lower bound, not a full decomposition. In
401 the evaluation-methodology line of Jordan et al. [3], O’Bray et al. [2], Paleka et al. [1], FA papers
402 should report BP-reference validity, layerwise credit quality, and a frozen-blocks depth-utilization
403 baseline as separate axes, not a single headline.

404 **Open questions and concrete next experiments.** The mechanism story in Section 4 treats Mode 1
405 as a plausible downstream symptom of Mode 2 rather than a parallel, independently destructive
406 failure, but the audit data is also formally consistent with a fully parallel reading. A direct test would
407 measure per-block forward-state-change content along the training trajectory and check whether
408 per-block decrease in test loss tracks per-block credit usefulness (e.g. nudging-test loss change)
409 more tightly than it tracks per-block angular agreement with the BP gradient; a complementary
410 test would substitute the random feedback B_l with a high-quality credit signal (sparse, learned to
411 predict the BP gradient, or weight-transport-restored à la Akrouit et al. [6]) at fixed $\|f_l\|$ and check
412 whether activation growth still appears, which would falsify the Mode 2 \rightarrow Mode 1 reading by
413 exhibiting Mode 1 in the absence of Mode 2. Beyond the mechanism question, a wider-scope
414 replication would extend the same audit to additional datasets (CIFAR-100, Tiny-ImageNet) and
415 architectures outside the residual ResMLP / ViT-Mini family, which would calibrate how broadly
416 the protocol’s binary detectors generalize past the audited regime. The reference implementation in
417 Appendix A is intended to support such extensions at the level of training-recipe and architecture-
418 class configuration so the audit pipeline itself does not need to be re-derived.

419 References

- 420 [1] Daniel Paleka, Shashwat Goel, Jonas Geiping, and Florian Tramèr. Pitfalls in evaluating lan-
421 guage model forecasters. In *International Conference on Learning Representations*, 2026.
- 422 [2] Leslie O’Bray, Max Horn, Bastian Rieck, and Karsten M. Borgwardt. Evaluation metrics for
423 graph generative models: problems, pitfalls, and practical solutions. In *International Confer-
424 ence on Learning Representations*, 2022.
- 425 [3] Scott Jordan, Yash Chandak, Daniel Cohen, Mengxue Zhang, and Philip Thomas. Evaluat-
426 ing the performance of reinforcement learning algorithms. In *International Conference on
427 Machine Learning*, 2020.
- 428 [4] Timothy P. Lillicrap, Daniel Cownden, Douglas B. Tweed, and Colin J. Akerman. Random
429 synaptic feedback weights support error backpropagation for deep learning. *Nature Communi-
430 cations*, 7:13276, 2016.
- 431 [5] Arild Nøkland. Direct feedback alignment provides learning in deep neural networks. In
432 *Advances in Neural Information Processing Systems*, 2016.
- 433 [6] Mohamed Akrouit, Collin Wilson, Peter C. Humphreys, Timothy P. Lillicrap, and Douglas B.
434 Tweed. Deep learning without weight transport. In *Advances in Neural Information Processing
435 Systems*, 2019.
- 436 [7] Julien Launay, Iacopo Poli, François Boniface, and Florent Krzakala. Direct feedback align-
437 ment scales to modern deep learning tasks and architectures. In *Advances in Neural Informa-
438 tion Processing Systems*, 2020.
- 439 [8] Sergey Bartunov, Adam Santoro, Blake A. Richards, Luke Marris, Geoffrey E. Hinton, and
440 Timothy P. Lillicrap. Assessing the scalability of biologically motivated deep learning algo-
441 rithms and architectures. In *Advances in Neural Information Processing Systems*, 2018.

- 442 [9] Benjamin Scellier and Yoshua Bengio. Equilibrium propagation: bridging the gap between
 443 energy-based models and backpropagation. *Frontiers in Computational Neuroscience*, 11:24,
 444 2017.
- 445 [10] Theodore H. Moskovitz, Ashok Litwin-Kumar, and L. F. Abbott. Feedback alignment in deep
 446 convolutional networks. *arXiv preprint arXiv:1812.06488*, 2018.
- 447 [11] Maria Refinetti, Stéphane d’Ascoli, Ruben Ohana, and Sebastian Goldt. Align, then memorise:
 448 the dynamics of learning with feedback alignment. In *International Conference on Machine*
 449 *Learning*, 2021.
- 450 [12] Brian Crafton, Abhinav Parihar, Evan Gebhardt, and Arijit Raychowdhury. Direct feedback
 451 alignment with sparse connections for local learning. *Frontiers in Neuroscience*, 13:525, 2019.
- 452 [13] Ruibin Xiong, Yunchang Yang, Di He, Kai Zheng, Shuxin Zheng, Chen Xing, Huishuai Zhang,
 453 Yanyan Lan, Liwei Wang, and Tie-Yan Liu. On layer normalization in the transformer archi-
 454 tecture. In *International Conference on Machine Learning*, 2020.
- 455 [14] Yoshua Bengio. How auto-encoders could provide credit assignment in deep networks via
 456 target propagation. *arXiv preprint arXiv:1407.7906*, 2014.
- 457 [15] Dong-Hyun Lee, Saizheng Zhang, Asja Fischer, and Yoshua Bengio. Difference target propaga-
 458 tion. In *European Conference on Machine Learning and Principles and Practice of Knowledge*
 459 *Discovery in Databases (ECML PKDD)*, 2015.
- 460 [16] Max Jaderberg, Wojciech M. Czarnecki, Simon Osindero, Oriol Vinyals, Alex Graves, David
 461 Silver, and Koray Kavukcuoglu. Decoupled neural interfaces using synthetic gradients. In
 462 *International Conference on Machine Learning*, 2017.

463 A Reference Implementation

464 We will release a reference implementation at [https://github.com/](https://github.com/REPO-URL-TO-BE-INSERTED)
 465 `REPO-URL-TO-BE-INSERTED`. The release is intended to make the evaluation protocol easy
 466 to run and difficult to misreport: it contains one command path for training or loading checkpoints,
 467 one command path for computing the four diagnostics, and one command path for rendering the
 468 audit tables and figures used in the paper. The reference code should be treated as part of the
 469 evaluation artifact rather than as an auxiliary convenience, because several of the failure cases in
 470 this paper arise from seemingly minor choices in how gradients, layers, and baselines are measured.

471 The repository is organized around the claims in the paper rather than around model classes. A min-
 472 imal run should expose: (i) architecture-matched trainable-block and random-block baselines, (ii)
 473 per-layer residual-scale and BP-gradient measurements at fixed checkpoints, (iii) deep-layer cosine
 474 computations with the exact batch and masking conventions used by the audit, and (iv) summary
 475 scripts that emit the tables underlying Table 1, Table 2, and Table 3. The goal is that an outside
 476 reader can reproduce both the verdict and the reason for the verdict from a single checkpoint bundle
 477 without reverse-engineering hidden notebook logic.

478 B Pipeline Pitfalls Catalog

479 **Pitfall 1: Layer-0 dominance hidden by global averaging.** A single global cosine can look
 480 mildly positive even when all deep trainable blocks are effectively null, because the shallowest layer
 481 dominates the norm budget. The protocol therefore treats layerwise inspection as mandatory and
 482 interprets any aggregate headline only after checking where the signal comes from.

483 **Pitfall 2: Cosine against a numerical-floor BP reference.** If the deepest BP gradient norm has
 484 collapsed, the cosine to that vector is not a trustworthy direction-quality measurement. This is the
 485 core measurement-degeneracy failure, and it is why the protocol records $\|g_L\|$ before interpreting
 486 any deep-layer alignment statistic.

487 **Pitfall 3: Batch mismatch between reference and candidate gradients.** Using different mini-
488 batches, different augmentations, or different dropout masks for BP and FA credit vectors can inflate
489 or destabilize the reported cosine. The reference implementation computes both vectors on the same
490 frozen forward pass whenever the claim being tested is directional agreement rather than training
491 robustness.

492 **Pitfall 4: Baseline mismatch for depth utilization.** Comparing a partially trainable model only
493 to full BP or to an unmatched random baseline can make weak methods look stronger than they are.
494 Diagnostic (d) uses architecture-matched frozen-blocks controls precisely so that “the deep blocks
495 helped” is tested against the right null.

496 **Pitfall 5: Silent train/eval mode inconsistencies.** Small mode mismatches can change residual
497 scale, normalization behavior, and therefore the diagnostic measurements themselves. The measure-
498 ment scripts fix model mode explicitly and log it, because otherwise a paper can end up comparing
499 training-time FA credit with evaluation-time BP references.

500 **Pitfall 6: Post-hoc normalization that erases scale pathology.** Renormalizing hidden states or
501 gradients before logging can make a genuine activation-growth failure disappear from the report. For
502 this paper, raw norms are part of the scientific object, so any normalization used for visualization
503 must remain separate from the values used for diagnosis.

504 **Pitfall 7: Missing null controls for intervention claims.** A rescue intervention can improve co-
505 sine or accuracy for trivial reasons unless the experiment includes a null such as fresh- B feedback or
506 a matched BP+penalty control. The paper therefore treats intervention evidence as incomplete unless
507 it separates training-specific adaptation from generic regularization or capacity effects [8, 10, 11].

508 C Walk-Back Chain Methodology

509 The walk-back chain is the compressed narrative used to translate a superficially positive headline
510 result into a falsifiable diagnostic verdict. It has four steps. Step 1 asks what the status-quo claim
511 would be from accuracy and headline Γ alone. Step 2 checks whether the deepest hidden-layer BP
512 reference remains numerically meaningful; if not, the alignment claim is walked back as ungrounded
513 measurement. Step 3 asks whether trained deep blocks outperform architecture-matched random-
514 block baselines; if not, the training claim is walked back as unused or weakly used depth. Step 4 uses
515 temporal replay, intervention, and cross-architecture evidence to determine whether the underlying
516 problem is primarily measurement degeneracy, low intrinsic credit-direction quality, or both.

517 This chain is deliberately asymmetric. A method can pass all four steps and remain provisionally
518 trustworthy, but failing any one of the binary detectors is enough to invalidate the stronger claim
519 that “deep local credit assignment is working” on that setting. That asymmetry matches the paper’s
520 goal: not to certify methods as universally good, but to prevent unsupported success claims from
521 surviving because the reporting pipeline asked too little of the evidence.

522 D All Seven Validations

523 Table 4 lists the seven validation exercises that support the protocol. They serve different purposes:
524 some validate binary detection, some validate interpretation, and some validate external usefulness.
525 Together they show that the protocol is not merely a post-hoc description of one final ResMLP
526 run, but a portable evaluation procedure that changes conclusions across time, interventions, and
527 architectures.

528 A useful way to read the table is that no single validation carries the paper by itself. The five-
529 method audit shows that the problem exists, temporal replay shows that the protocol is actionable,
530 intervention and null controls show that the two modes respond differently, and cross-architecture
531 evidence shows which parts of the protocol are specific to terminal-normalized residual settings and
532 which parts are more general.

Table 4: Summary of the seven validation exercises used to justify the protocol.

Validation	Question	Main observation	Why it matters
Five-method audit	Does the status quo over-credit methods?	Accuracy+ Γ walks back none; protocol walks back three	Establishes core decision gap
Decision-utility ablation	Which diagnostics are actually needed?	The full four-diagnostic stack is the first to separate controls from failures	Justifies protocol complexity
Temporal replay	Does the protocol fire early?	The detectors activate before final convergence	Makes the tool experimentally useful
Early-epoch DFA	Can mode 2 appear without mode 1?	Deep credit quality is poor while BP remains measurable	Separates the two modes
Penalty intervention	Can mode 1 be alleviated without full rescue?	Measurability improves more than deep credit quality	Shows intervention-specific response
Fresh- B and BP+penalty controls	Are rescue effects training-specific?	Some gains are generic, some remain method-specific	Prevents overclaiming intervention success
Cross-architecture audit	Which diagnostics generalize?	Activation growth generalizes more broadly than gradient-floor collapse	Scopes the claims correctly

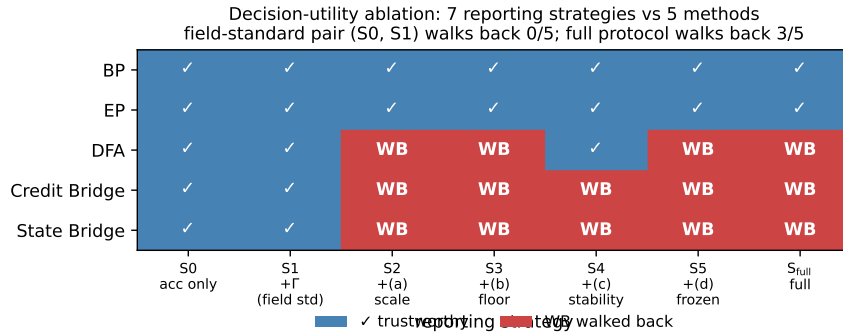


Figure 6: Decision-utility ablation (seven reporting strategies \times five methods) supporting Section 6: accuracy alone and accuracy+ Γ walk back 0/5 audited methods, while any one of the diagnostics (a), (b), or (d) already walks back the three silent failures; the full four-diagnostic protocol also walks back 3/5. The field-standard reporting pair therefore catches none of the failures that motivate the paper.

533 E Threshold Sensitivity Full Sweep

534 The sensitivity sweep is intentionally small because the paper does not claim that all four thresholds
 535 are equally canonical. The important result is qualitative stability for diagnostics (a) and (b): over a
 536 reasonable range of nearby cutoffs, the same methods are flagged on the same audited settings, and
 537 the same controls remain unflagged. This is the strongest calibration evidence in the paper because
 538 these two diagnostics track the physical quantities most directly tied to the measurement-degeneracy
 539 story.

540 Diagnostic (d) is weaker and should be presented that way. Its threshold is best understood as
 541 a conservative reporting aid for depth utilization rather than as a universal constant. In practice,
 542 the full sweep should therefore be read as showing that the protocol is robust where it claims binary
 543 detection strength and intentionally modest where it is used as a contextual check on whether trained
 544 deep blocks beat architecture-matched random-block baselines.

545 **F Per-Architecture Detailed Audits**

546 The per-architecture appendix should be short and comparative. On pre-LayerNorm ResMLP and
 547 ViT-Mini, the key pattern is the same as in the main text: residual-scale growth can become large
 548 enough that the deepest BP reference becomes numerically weak, and the status-quo pair of accuracy
 549 plus headline Γ fails to expose that. These are the settings where both failure modes matter and
 550 where the full protocol is most necessary.

551 The no-terminal-LN ResMLP ablation and the CNN serve a different role. They test whether the
 552 protocol overgeneralizes from terminal-normalized residual architectures to settings where gradient-
 553 floor collapse is not expected. In those models, activation-growth checks can still reveal weak depth
 554 usage or poor scaling, but diagnostic (b) is not expected to fire in the same way. This asymmetry is
 555 not a weakness of the protocol; it is part of the empirical scoping claim of the paper and helps prevent
 556 readers from mistaking a targeted evaluation standard for a universal pathology claim [13, 8].

557 **G Depth-Sweep Layerwise Profiles**

558 To check whether the layerwise pattern in Figure 1 is an artifact of the specific four-block depth
 559 used in the main audit, we ran the same architecture on $d=512$ pre-LayerNorm ResMLPs at five
 560 depths $L \in \{2, 4, 6, 8, 12\}$ on CIFAR-10 (single seed 42, otherwise matched configuration). Table 5
 561 reports the layer-0 cosine, the mean cosine over all deeper layers, and the deep mean perturbation
 562 correlation ρ for each depth.

Table 5: Depth sweep on $d=512$ ResMLP, seed 42, 100 epochs CIFAR-10. *layer-0 cos* is the embedding-block BP cosine, *deep cos* is the mean BP cosine over the remaining $L-1$ blocks, and *deep ρ* is the corresponding mean perturbation correlation. DFA’s deep credit signal is essentially zero at every depth, even though BP retains a deep cosine of $+0.94$ at $L=12$.

L	method	test acc	layer-0 cos	deep cos	deep ρ
2	BP	0.599	+1.000	+1.000	+0.983
2	DFA	0.312	+0.396	-0.005	+0.000
2	Credit Bridge	0.310	+0.330	+0.020	+0.000
4	BP	0.603	+1.000	+1.000	+0.988
4	DFA	0.314	+0.400	-0.000	+0.000
4	Credit Bridge	0.298	+0.402	+0.030	+0.000
6	BP	0.602	+0.993	+0.993	+0.991
6	DFA	0.310	+0.387	-0.000	+0.000
6	Credit Bridge	0.299	+0.304	+0.054	+0.000
8	BP	0.589	+0.965	+0.965	+0.992
8	DFA	0.306	+0.377	-0.000	+0.000
8	Credit Bridge	0.288	+0.205	+0.022	+0.000
12	BP	0.594	+0.942	+0.940	+0.990
12	DFA	0.309	+0.388	-0.000	+0.000
12	Credit Bridge	0.239	+0.208	+0.016	+0.000

563 The layerwise pattern is essentially depth-invariant. DFA’s layer-0 cosine stays in $[+0.38, +0.40]$
 564 across all five depths, while its mean deep cosine sits within $[-0.005, +0.000]$ and its deep ρ col-
 565 lapses to numerical zero in every condition. Credit Bridge shows a slightly milder version of the
 566 same shape, with a small positive deep cosine that does not improve as depth shrinks. BP, by
 567 contrast, maintains a deep cosine of $+0.94$ even at $L=12$, so the BP reference is still measurably
 568 non-degenerate where DFA and Credit Bridge are flat. The $L=4$ row, which matches the main au-
 569 dit’s architecture, has also been replicated across three seeds (42, 123, 456): 3-seed DFA layer-0
 570 cosine is $+0.412 \pm 0.011$, 3-seed DFA deep cosine is -0.0004 ± 0.0008 , and 3-seed CB deep cosine
 571 is $+0.039 \pm 0.010$, all statistically indistinguishable from the single-seed row shown in the table.
 572 This rules out the explanation that DFA’s deep blocks are merely too far from the loss to receive
 573 useful credit: making the network shallower does not reach the deep blocks any better. The failure
 574 is structural to the credit signal rather than an artifact of depth.

575 **H No-Residual Ablation: Skip Path Is Not the Proximate Trigger**

576 To test whether Mode 1 is specifically a property of the additive residual skip $h_{l+1} = h_l + F_l(h_l)$, we
 577 ran a matched ablation on the same 4-block $d=256$ ResMLP, on CIFAR-10, with the same optimizer,
 578 learning rate, weight decay, batch size, and seed (42), but replaced each block by $h_{l+1} = F_l(h_l)$ and
 579 increased the inner w_2 initialization standard deviation from 0.01 to 0.5 to make the no-residual
 580 stack trainable from step zero. Terminal LayerNorm and the rest of the architecture are unchanged.
 581 Three-epoch smoke results:

Table 6: No-residual ResMLP-d256 ablation, seed 42, 3 epochs each. Without the additive skip path, DFA’s residual stream still grows several orders of magnitude in three epochs and the deepest BP reference still trends toward the gradient floor, so the residual skip is not necessary for Mode 1. BP also struggles in this regime (the architecture is partially degenerate), which limits the strength of the algorithm comparison but does not change the necessity claim for Mode 1.

method	w_2 std	ep	$\ h_L\ $	$\ g_L\ $	test acc	gamma_dfa
BP	0.5	0	4.69	9.8×10^{-4}	0.080	—
BP	0.5	1	155	4.3×10^{-5}	0.144	—
BP	0.5	2	174	4.0×10^{-5}	0.164	—
BP	0.5	3	163	4.2×10^{-5}	0.163	—
DFA	0.5	0	4.69	9.8×10^{-4}	0.080	—
DFA	0.5	1	5,295	8.6×10^{-7}	0.156	0.047
DFA	0.5	2	16,930	2.2×10^{-7}	0.151	0.040
DFA	0.5	3	22,050	1.6×10^{-7}	0.148	0.039

582 The qualitative shape matches what we see in vanilla residual DFA, only with a slower onset because
 583 the architecture itself is harder to train. Diagnostic (a) clearly fires within three epochs, and diag-
 584 nostic (b) is already on the floor side of 10^{-7} . Across w_2 std values $\{0.1, 0.2, 0.5\}$ that we tried in
 585 the same smoke sweep, the qualitative outcome is the same: residual stream grows by three to four
 586 orders of magnitude, $\|g_L\|$ drops by three to four orders of magnitude, and BP itself never reaches a
 587 healthy training regime. We retain $w_2=0.5$ here because that is the only value where BP is at least
 588 beginning to learn. The full 100-epoch trajectory of the same configuration, replicated across three
 589 seeds (42, 123, 456), converges to a mean $\|h_L\| \approx 8.2 \times 10^7$ and mean $\|g_L\| \approx 1.9 \times 10^{-10}$ (per-
 590 seed values $\|h_L\| \in \{1.06 \times 10^8, 3.15 \times 10^7, 1.09 \times 10^8\}$ and $\|g_L\| \in \{1.08, 2.94, 1.77\} \times 10^{-10}$),
 591 all deeply below the diagnostic (b) floor and within an order of magnitude of vanilla residual DFA’s
 592 three-seed mean $\|h_L\| \approx 5 \times 10^8$ and mean $\|g_L\| \approx 4 \times 10^{-10}$ on the same backbone, confirming
 593 that the smoke-test trend is the converged behavior rather than an early-training artifact.

594 We treat this ablation as evidence about *necessity*, not about clean algorithm separation. Specifically,
 595 the evidence supports: the additive residual skip is not necessary for Mode 1 activation growth
 596 or for the gradient-floor trend; Mode 1 (a) appears to be a generic deep-DFA instability on these
 597 stacks, modulated but not gated by skip presence; and the catastrophic, well-defined $\|g_L\|$ collapse
 598 remains most tightly associated with terminal LayerNorm in our audited settings, where the no-
 599 out_In control already showed activation growth without the same severity of collapse. The full
 600 100-epoch trajectory of this no-residual run is reported as a confirmatory check rather than as a
 601 primary claim.

602 **I Random-Target Ablation: Mode 1 Is Data-Agnostic**

603 To test whether Mode 1 activation growth requires any task signal at all, we re-ran DFA on the stan-
 604 dard 4-block $d=256$ pre-LayerNorm ResMLP, on CIFAR-10 inputs, but replaced each minibatch’s
 605 labels with i.i.d. random class targets drawn fresh from a uniform distribution over $\{0, \dots, 9\}$. All
 606 other hyperparameters are matched to the vanilla DFA training run in Section 2 (AdamW, lr= 10^{-3} ,
 607 wd= 0.01, 128 batch, cosine schedule, single seed 42 for the smoke test). The local feedback vectors
 608 B_l are unchanged. Three-epoch trajectory:

609 This ablation answers the natural counterargument that DFA’s residual-stream growth might be a
 610 side-effect of the network adapting to genuine task signal in a particularly bad local minimum: it
 611 is not. With no task signal at all, DFA on this architecture still inflates the residual stream by more

Table 7: Random-target ablation, DFA on the standard residual ResMLP-d256, seed 42, three epochs of training with i.i.d. random class targets refreshed every minibatch. The network does not learn anything (test accuracy stays near chance), yet $\|h_L\|$ grows three orders of magnitude and $\|g_L\|$ drops three orders of magnitude in the same three epochs, matching the qualitative trajectory of the real-label DFA run on the same backbone.

ep	$\ h_L\ $	$\ g_L\ $	test acc	gamma_dfa
0	8.89	9.83×10^{-4}	0.115	—
1	1,616	5.12×10^{-6}	0.078	-0.020
2	9,768	8.50×10^{-7}	0.081	-0.024
3	14,510	5.62×10^{-7}	0.071	-0.025

612 than three orders of magnitude in the first three epochs and pushes the deepest BP reference gradient
613 to the floor of 10^{-7} in the same window. The full 100-epoch trajectory of the same DFA random-
614 target run converges to $\|h_L\| \approx 1.67 \times 10^8$ and $\|g_L\| \approx 8.0 \times 10^{-12}$, both more extreme than
615 the corresponding endpoints of vanilla DFA on the same backbone with real labels (about 4×10^8
616 and 5×10^{-10} respectively), so the data-agnostic trajectory does not just reach Mode 1 but in fact
617 passes through the same regime even without any per-sample task pressure. The local DFA objective
618 $\langle f_l(h_l), e_T B_l^T \rangle$ contains no penalty on $\|f_l(h_l)\|$, so any direction in which a larger block output
619 increases inner-product alignment with the fixed feedback target is rewarded; the random-target run
620 isolates exactly this geometric incentive, free of any task-driven feature pressure. The full 100-epoch
621 trajectory of this random-target run is reported as a confirmatory check rather than a primary claim.

622 We then asked whether this data-agnostic growth is specific to DFA or generalizes to other fixed-
623 feedback local-credit methods, by repeating the random-target ablation under State Bridge and
624 Credit Bridge with the same architecture, hyperparameters, and seed. Both methods also exhibit
625 data-agnostic activation growth in the same three-epoch window, with $\|h_L\|$ rising from about 9 to
626 about 6.2×10^3 (State Bridge) and about 2.0×10^4 (Credit Bridge), while their test accuracies remain
627 at chance (0.10 and 0.09, respectively):

Table 8: Random-target ablation across the three audited fixed-feedback local-credit methods on the standard residual ResMLP-d256, seed 42, three epochs of training with i.i.d. random class targets. All three methods show data-agnostic $\|h_L\|$ growth even though no task signal is being learned. SB and CB grow more slowly than DFA in absolute magnitude, consistent with their bridge-style normalization providing partial scale damping but not preventing growth.

method	$\ h_L\ $ at ep 3	$\ g_L\ $ at ep 3	test acc
DFA	14,510	5.6×10^{-7}	0.071
State Bridge	6,225	1.0×10^{-5}	0.104
Credit Bridge	19,974	3.2×10^{-6}	0.092

628 The cross-method version of the test rules out the explanation that the random-target growth is
629 specific to DFA’s particular feedback projection. State Bridge and Credit Bridge use bridge con-
630 structions with target normalization and stop-gradients, so any residual-stream growth they exhibit
631 cannot be attributed to a simple absence of normalization. Their $\|g_L\|$ values at three epochs are
632 still well above the 10^{-7} floor used by diagnostic (b), so the gradient collapse part of Mode 1 does
633 not yet appear at this horizon for SB/CB; the activation-growth part of Mode 1 is already present.
634 At the full 100-epoch trajectory of the same random-target protocol, both SB and CB also reach
635 the (b) floor: SB converges to $\|h_L\| \approx 3.6 \times 10^5$ and $\|g_L\| \approx 4 \times 10^{-8}$, and CB converges to
636 $\|h_L\| \approx 1.38 \times 10^8$ and $\|g_L\| \approx 0$ (below the numerical clamp), with test accuracies 0.100 and
637 0.085 respectively, consistent with DFA’s 1.67×10^8 and 8.0×10^{-12} at the same horizon. We
638 treat this as evidence that the local-credit growth incentive is not unique to DFA but is shared by the
639 audited family of fixed-feedback methods.

640 The cleanest negative control for the random-target assay is Equilibrium Propagation, which trains
641 the same backbone with a contrastive nudged-vs-free local energy objective rather than a fixed feed-
642 back projection. We re-ran EP on the same ResMLP-d256 with i.i.d. random class targets, seed 42,
643 identical hyperparameters: EP’s $\|h_L\|$ stays at about 557 at five epochs of training and converges to
644 about 2,151 over the full 100-epoch trajectory (median over $n=2048$ test inputs, model in eval mode;

645 see results/ep_random_h_L_summary.json), which is roughly $26\times$ smaller than DFA’s 14,510
 646 at three epochs and is in the same range as vanilla EP’s bounded trajectory on real labels ($\sim 5 \times 10^3$).
 647 At convergence, the random-target EP run reaches headline accuracy 0.081, headline $\Gamma = -0.0003$,
 648 and headline $\rho = -0.006$, all consistent with chance-level performance and a non-degenerate mea-
 649 surement regime. The random-target assay therefore separates the audited fixed-feedback methods
 650 (DFA/SB/CB) from EP cleanly: fixed-feedback objectives without an explicit scale-control term ex-
 651 hibit data-agnostic activation growth on this architecture, while EP’s energy-based local objective
 652 does not.

653 J State Bridge and Credit Bridge Penalty Rescue: 3-Seed Cross-Method 654 Test

655 To test whether the per-block scale-control penalty $\lambda \text{mean}(\|f_l(h_l)\|^2)$ that rescues DFA in Section 5
 656 also rescues other audited fixed-feedback local-credit methods, we re-ran State Bridge and Credit
 657 Bridge on the standard 4-block $d=256$ pre-LayerNorm ResMLP for 30 epochs and three seeds (42,
 658 123, 456), with $\lambda=10^{-2}$ added to each method’s per-block local loss only (the bridge state predictor,
 659 the bridge value network, and the embedding/head paths are not penalized, matching the DFA rescue
 660 setup). We also ran matched vanilla State Bridge and Credit Bridge baselines at seed 42 with the
 661 same architecture and training schedule but $\lambda=0$. Three-seed converged values:

Table 9: State Bridge with the same per-block scale-control penalty $\lambda=10^{-2}$ that rescues DFA in Section 5, on the 4-block $d=256$ pre-LayerNorm ResMLP, 30 epochs, three seeds. SB+penalty reaches a converged test accuracy of 0.453 ± 0.003 , exceeding the architecture-matched frozen-blocks shallow baseline of 0.349 by +10.4 percentage points and the matched 30-epoch DFA+penalty value of 0.360 ± 0.001 by +9.3 percentage points. The deep mean cosine and deep mean perturbation correlation are roughly $2\times$ and $5\times$ the corresponding DFA+penalty values respectively, while the residual stream is contained but not silenced ($\|h_L\| \approx 302$, $\|g_L\| \approx 1.8 \times 10^{-4}$). Vanilla SB on the same architecture and seed reaches only 0.213, with $\|h_L\| \approx 9.85 \times 10^6$ and $\|g_L\|$ at the diagnostic-(b) floor.

seed	test acc	$\ h_L\ $	$\ g_L\ $	deep cos	deep ρ
SB+pen 42	0.4564	302	1.75×10^{-4}	+0.312	+0.392
SB+pen 123	0.4514	311	1.74×10^{-4}	+0.327	+0.424
SB+pen 456	0.4509	292	1.92×10^{-4}	+0.326	+0.391
SB+pen mean	0.453 ± 0.003	302 ± 8	1.80×10^{-4}	$+0.322 \pm 0.007$	$+0.402 \pm 0.015$
CB+pen 42	0.3596	5431	1.88×10^{-5}	+0.684	+0.498
CB+pen 123	0.3642	5834	1.81×10^{-5}	+0.667	+0.452
CB+pen 456	0.3562	5775	2.01×10^{-5}	+0.685	+0.442
CB+pen mean	0.360 ± 0.003	5680 ± 178	1.90×10^{-5}	$+0.679 \pm 0.008$	$+0.464 \pm 0.025$
vanilla SB 42	0.213	9.85×10^6	1×10^{-8}	—	—
vanilla CB 42	0.211	6.7×10^7	~ 0	—	—
DFA+pen mean	0.360 ± 0.001	1.3×10^4	1.6×10^{-6}	$+0.151 \pm 0.025$	$+0.080 \pm 0.011$

662 The penalty rescue effect on State Bridge is much larger than on DFA: +24 percentage points for
 663 State Bridge versus +5.9 percentage points for DFA on the same architecture and intervention.
 664 SB+penalty is the first audited non-BP method whose trained deep blocks substantively beat the
 665 architecture-matched random-block baseline. We treat this as evidence that Mode 2 (low intrinsic
 666 credit-direction quality) has method-dependent severity within the audited fixed-feedback family
 667 once Mode 1 is alleviated, rather than being a uniform property of all fixed-feedback local-credit ob-
 668 jectives. Importantly, State Bridge’s deep cosine +0.322 is approximately twice DFA’s +0.151 on
 669 the same intervention, but neither approaches the BP reference value of $\approx +1.0$, so this is a within-
 670 class gradation in credit-direction quality, not a claim that bridge constructions “solve” Mode 2.
 671 The drift diagnostic reinforces this reading rather than contradicting it: per-block w_2 relative dis-
 672 placement after 30 epochs averages $14.8 \times \pm 0.5$ for SB+penalty, $18.6 \times \pm 0.5$ for DFA+penalty, and
 673 $19.1 \times \pm 0.6$ for CB+penalty (three seeds each), and the embedding layer’s relative drift is $7.0 \times \pm 0.1$
 674 for SB versus $46.3 \times \pm 1.5$ for CB and $94.6 \times \pm 1.4$ for DFA, so none of the three methods’ per-block
 675 updates are silenced under penalty and CB’s are in fact larger in magnitude than SB’s while DFA’s

676 embedding updates are the largest of all, yet CB’s and DFA’s final accuracies are both 9.3 percent-
677 age points below State Bridge’s. The larger-but-less-useful parameter updates in CB are consistent
678 with the mechanism hypothesis that angular agreement with the BP gradient does not by itself cer-
679 tify the functional forward-state content of the update. The nudging test at the same checkpoints
680 provides the direct functional measurement: taking a single step of size $\eta=0.01$ in the direction of
681 each method’s per-layer credit a_l at the converged checkpoint and measuring the resulting test-loss
682 change averaged over the deep blocks (11–13 of the 4-block model) gives, across three seeds (42, 123,
683 456), $-1.93 \pm 0.11 \times 10^{-3}$ for SB+penalty (per-seed deep means $\{-1.78, -1.96, -2.05\} \times 10^{-3}$),
684 $-4.26 \pm 0.24 \times 10^{-4}$ for CB+penalty (per-seed $\{-4.45, -3.93, -4.42\} \times 10^{-4}$), and $-4.98 \pm$
685 0.44×10^{-5} for DFA+penalty (per-seed $\{-5.53, -4.46, -4.95\} \times 10^{-5}$). At the same per-layer
686 credit direction, a step in SB’s direction moves the loss about $4.5\times$ more than a step in CB’s di-
687 rection and about $39\times$ more than a step in DFA’s direction, even though CB’s direction is more
688 aligned with the BP gradient in angle than either. The full per-seed per-block nudging values
689 are saved in `results/nudging_test_3seed_summary.json`. The 30-epoch training trajectories
690 give a third independent confirmation: across three seeds, SB+penalty’s training loss decreases by
691 0.447 ± 0.008 over the run (per seed $\{0.457, 0.444, 0.439\}$), whereas CB+penalty’s decreases by
692 only 0.121 ± 0.003 (per seed $\{0.123, 0.118, 0.124\}$) and DFA+penalty’s by only 0.095 ± 0.007
693 (per seed $\{0.104, 0.088, 0.093\}$). Deep cosine ranks the three methods $CB > SB > DFA$, but every
694 functional metric (nudging, integrated training-loss decrease, headline accuracy) ranks them $SB \gg$
695 $CB \approx DFA$: the ordering produced by deep cosine is the only one that does not predict accuracy
696 correctly. This is the strongest form of the cos-versus-accuracy dissociation: across three audited
697 fixed-feedback methods under the same penalty intervention, the ranking implied by angular agree-
698 ment with the BP gradient is contradicted by three independent functional measurements that do
699 predict accuracy. Under the same intervention Credit Bridge reaches a three-seed test accuracy of
700 0.360 ± 0.003 , a three-seed deep mean cosine of $+0.679 \pm 0.008$, and a three-seed deep mean ρ of
701 $+0.464 \pm 0.025$, with $\|h_L\| \approx 5680 \pm 178$ and $\|g_L\| \approx 1.9 \times 10^{-5}$ well above the diagnostic floor.
702 Credit Bridge therefore has an even higher deep cosine than State Bridge (about $4\times$ the DFA value
703 and roughly $2\times$ the State Bridge value), but reaches the same final accuracy as DFA+penalty and
704 9.3 percentage points below State Bridge+penalty. This is a clean dissociation: within the audited
705 fixed-feedback family under the same rescue, deep cosine and deep ρ differ by more than a factor
706 of four across methods without tracking final accuracy in the same direction, so alignment to the BP
707 gradient is a necessary but not sufficient diagnostic of usable credit for depth. That cross-method
708 dissociation is a direct reason the protocol in Section 6 keeps final accuracy, layerwise credit quality,
709 and the depth-utilization baseline as three separate reporting axes rather than collapsing them into a
710 single headline.

711 K Layer-0 Dominance: Per-Seed Vanilla DFA Early-Epoch Cosines

712 For the layer-0-dominance claim in Section 4, the per-layer cosines between DFA’s local credit
713 signal $a_l = e_T B_l^T$ and the BP gradient at the corresponding hidden state were measured
714 on the saved vanilla DFA early-epoch checkpoints (Section 4, Table 2). All measurements
715 use the script’s default eval batch ($n=2048$ CIFAR-10 test samples) and the training-time B_l
716 matrices reconstructed from the original training RNG. Layer indices follow the convention
717 used elsewhere in the paper: $l=0$ is the first residual block (which sees the embedding out-
718 put) and $l=1..4$ are the deeper residual blocks. The full per-seed values are dumped to
719 `results/vanilla_dfa_early_ckpts/per_layer_cos_3seed.json`.

720 The deep-layer mean across the three seeds at epoch 1 is -0.008 ± 0.013 (matching Table 2), and
721 at epoch 2 is -0.018 ± 0.018 . Layer 0 stays at $+0.42 \pm 0.02$ across all six measurements, so the
722 layer-0-dominance pattern is not a single-seed coincidence: it is consistent across seeds and across
723 the early epochs in which $\|g_2\|$ remains above the 10^{-7} diagnostic-(b) floor. This is the per-seed
724 evidence behind the Section 4 claim that aggregate cosine on vanilla DFA can look mildly positive
725 only because layer 0 carries the entire alignment budget.

726 L Reproducibility

727 All headline audit results in the main text should be reported over the locked seed set $\{42, 123, 456\}$,
728 with the same seed bundle reused across methods wherever possible so that between-method com-

Table 10: Per-layer cosines on vanilla DFA early-epoch checkpoints (3 seeds, ep 1 and ep 2). Layer 0 is consistently $\approx +0.42$ across all six measurements while every deep layer (1–4) lies in $[-0.06, +0.02]$, so the headline aggregate Γ on these checkpoints is driven almost entirely by layer 0 even though the deep blocks carry essentially no alignment with the BP gradient.

seed	ep	$l=0$	$l=1$	$l=2$	$l=3$	$l=4$	$\ g_2\ $
42	1	+0.421	+0.005	-0.028	-0.039	-0.038	6.8×10^{-7}
42	2	+0.437	-0.002	-0.040	-0.055	-0.054	1.6×10^{-7}
123	1	+0.436	+0.008	-0.033	+0.016	+0.017	6.6×10^{-7}
123	2	+0.460	+0.005	-0.037	+0.003	+0.003	1.4×10^{-7}
456	1	+0.418	+0.011	-0.026	+0.007	+0.006	3.8×10^{-7}
456	2	+0.409	+0.003	-0.039	+0.001	+0.000	8.5×10^{-8}

729 parisons are not driven by different data orders or initialization luck. Every released result table
 730 should specify the architecture, optimizer, learning-rate schedule, batch size, augmentation recipe,
 731 number of epochs, checkpoint selection rule, and whether each diagnostic was measured at the final
 732 checkpoint or along a stored temporal trajectory.

733 Hyperparameters should be listed exactly as run, not reconstructed from memory after the fact. For
 734 intervention experiments, the appendix should report the penalty coefficient, where in the network
 735 the penalty is applied, and which control runs share the same added objective. For diagnostic scripts,
 736 reproducibility requires logging the model mode, minibatch identity, and layer-index convention
 737 used for per-layer statistics. The point of this appendix is simple: because the paper’s claims hinge
 738 on how evaluation is performed, measurement configuration is part of the result and must be repro-
 739 ducible with the same care as training configuration.